Elastic Interpretation of Unsaturated undrained Pressuremeter Tests in clays

J. Monnet
Gaiatech , 22 rue Antoine Chollier, Seyssinet F-38170, France ; monnet. jacques@wanadoo.fr

L. Boutonnier[1], D.Mahmutovic[2]
Egis Géotechnique, 3 Rue du Dr Schweitzer, F-38180, Seyssins; luc.boutonnier@egis.fr: dino.mahmutovic@egis.fr [2]

ABSTRACT: The purpose of this study is to solve for pressuremeter the passage of pressure measurements to basic mechanical quantities (E; c; Φ) with undrained conditions but interpreted in effective stress. This research takes into account the interstitial pressure and the effective stresses for an unsaturated undrained soil. Occluded air is mostly present in natural soils and its compressibility leads to a partial transfer of the total isotropic stresses on the skeleton during undrained stress, which changes for an important way the soil response to undrained stress. This paper presents the theoretical developments and numerical validation in the case of linear elasticity. This is a first step to interpret the pressuremeter test differently and more precisely. For small deformations into finite volume, this study shows the existence of large variations of interstitial pressures related to the variation of the average volume of soil around the pressuremeter.

Keywords: pressuremeter, undrained test, unsaturated soil, elastic interpretation

1. Introduction

In the field of civil engineering, the pressuremeter is widely used for the design of structures such as shallow foundations (Appendix D - [1]) or the settlement of foundations (Appendix H - [2]). These methods use the geotechnical characteristics of the soil related to the pressuremeter test, namely the Ménard p_{LM} limit pressure and the Ménard E_M pressuremeter module. It is now known that these quantities are not intrinsic characteristics of the soil and can not be introduced as data in a calculation by Finite Elements or Finite Differences for the study of civil engineering works (retaining walls, Tunnels, slope stability, Embankments ...). These modern calculation require at least the knowledge of the elastic characteristics of the soil (Young's modulus E, Poisson's ratio ν) and the shearing resistance (cohesion c, friction angle Φ).

This study assumes undrained conditions which are frequently encountered in practice, but interpreted in total stress so far [3-5]. The assumption of total stress test does not allow to reach the fundamental mechanical characteristics of the soil, because the effect of the sucking or the interstitial overpressure is integrated in the mechanical resistance of the soil to represent the test in an equivalent elastic body.

We propose in this paper to take into account the interstitial pressure and the effective stresses for an undrained unsaturated soil. Indeed, occluded air is mostly present in natural soils [6-7] and its compressibility leads to a partial transfer of the total isotropic stresses on the skeleton during an undrained stress, which significantly changes the response of the soil to undrained stress. In the interpretation of the pressuremeter, these phenomena remain to be taken into account. This paper presents the theoretical developments and numerical model validation in the case of linear elasticity. This is a first step to interpret the pressuremeter test differently and more precisely.

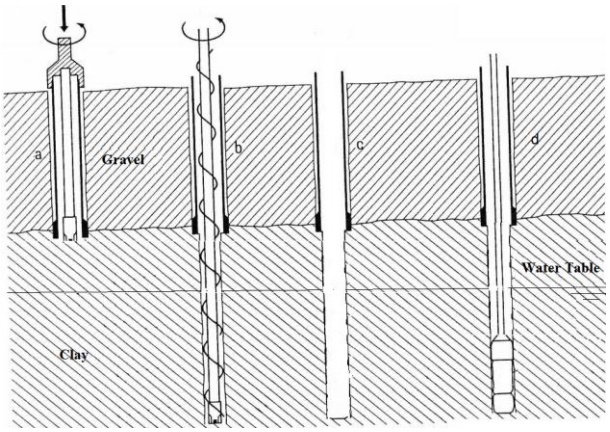

Figure 1. The main steps in carrying out the pressuremeter test

2. Theoretical model of undrained soil

2.1. The Ménard pressuremeter test

The Ménard pressuremeter test is carried out with a preliminary drilling (b, Fig. 1), possibly drilled after a prehole (a, Fig. 1). The auger is then removed from the borehole (c, Fig. 1), which has the effect of discharging the soil in horizontal stress, either under or above the water table. The unloading of the soil under the water table leads to a negative water pressure variation, which can go as far as the generation of suction. Then the probe (d, Fig. 1) is introduced and the test begins by progressively inflating until contact with the borehole. This phase partially restored the initial conditions in the soil, neglecting the 3D effects and if the unloading of the soil did not reaches plasticity. The test is continued

by increasing the total horizontal stress up to the limit pressure. This phase produces an increase in the interstitial pressure that we quantify in order to estimate an effective pressuremeter module.

2.2. The saturation domains proposed by Boutonnier [6-7]

The behavior of an unsaturated soil can be decomposed into 4 domains according to the degree of saturation.

2.2.1. Domain D1 : $s \geq s_{air}$ et $S_r \leq S_{rair}$

The gas phase is continuous in the soil. This state corresponds to suction greater than the air inlet suction and a degree of saturation lower than the saturation degree of air inlet. The degree of saturation of air inlet is often close to 90%.

2.2.2. Domain D2 : $s \leq s_{air}$ et $S_{rair} \leq S_r \leq S_{re}$

In this area, the free air has disappeared. The air is occluded in the soil. Suction increases the forces of interparticle contacts.

2.2.3. Domain D3 : $S_{re} < S_r < 1$ *et* $u_w > u_{we}$

The occluded air is considered as independent bubbles separated to the skeleton. The capillary tension, which exists on the surface of each bubble, has no effect on the contact forces between soil particles at the macroscopic scale. We consider that D3 corresponds to the case of positive interstitial pressures with S_r <1, which results in the assumption u_{we} = 0. The degree of saturation where the positive interstitial pressures appear is close to 96%

2.2.4. Domain D4 : $S_r = 1$

There is no air in the gaseous state in the soil sample under consideration. The soil is perfectly saturated. The boundary between D3 and D4 can also be expressed through the interstitial pressure u_{wsat} for which S_r = 1. This pressure is usually a few hundred kPa.

2.3. Mechanical behavior of unsaturated soils

2.3.1. Suction and effective stress

Suction has an effect on the effective stresses:

- in the saturated D4 and quasi-saturated D3 domains, there is no suction and the Therzaghi [8] eq. (1) applies

$$\sigma' = \sigma - u_w \quad (1)$$

- in the unsaturated D2 domain, there is a suction s and the eq. (2) applies

$$\sigma' = \sigma + s \quad (2)$$

- in the unsaturated D1 domain, the effective stress is given by eq. (3). We have χ <1 for suction greater than the air inlet suction; Terzaghi's theory no longer applies.

$$s = u_a - u_w \quad (3)$$

$$\sigma' = \sigma + \chi . s \quad (4)$$

2.4. Skempton [9] Coefficient B for Triaxial Test

In the undrained triaxial test Skempton [9] assumes eq. (5) that the variation of interstitial pressure Δu_w is composed into a variation Δu_i which depends on the average stress and a variation Δu_d which depends on the shear eq. (6).

The coefficient B of Skempton [9] relates the variation of interstitial pressure to the variation of total average pressure.

Using the Eq. of Terzaghi [8], Skempton [9] obtains for the triaxial test, with a compressibility of the soil skeleton c_{sol} and that of the interstitial fluid c_f, the expression of the coefficient B eq. (7) connecting the interstitial pressure Δu_i with the total mean pressure increase Δp

$$\Delta u_w = \Delta u_i + \Delta u_d \quad (5)$$

$$\Delta u_w = B.[\Delta\sigma_3 + A.(\Delta\sigma_1 - \Delta\sigma_3)] \quad (6)$$

$$\Delta u_i/\Delta p = B = 1/[1 + n.(c_f/c_{sol})] \quad (7)$$

2.5. Coefficient of compressibility c_f interstitial fluid

2.5.1. Definition of the compressibility coefficient c_f

For unsaturated soil, the interstitial fluid is composed of a mixture of water and air of very different compressibility. However, assuming a homogeneity of the air and water, we consider following Boutonnier, [6] the interstitial fluid as an equivalent compressible fluid. The definition of the compressibility coefficient c_f of the interstitial mixture of water and air bubbles is indicated in eq. (8) and can be found in [6].

$$c_f = -dV_v/(V_v.du_w) = -dV_v/(n.V_0.du_w) \quad (8)$$

It is obtained for unsaturated soils by the derivation of the degree of saturation S_r according to eq. (9) which is demonstrated in [10].

$$c_f = dS_r/(S_r.du_w) + c_w \quad (9)$$

2.5.2. Domain D2: the coefficient c_f is quasi-constant

In the D2 domain, Boutonnier [6] found that a simple linear expression between degree of saturation and suction allowed to model laboratory tests. This expression has been simplified by assuming a linear Eq.ship eq. (10) with water pressure [7]. The compressibility coefficient of the resulting air + bubble mixture is therefore almost constant with this assumption as illustrated in Fig. 2 and equation eq. (11).

$$S_r = S_{re} - u_w/u_{w\,air}.(S_{re} - S_{r\,air}) \quad (10)$$

$$c_f \approx -(S_{re} - S_{r\,air})/(S_r.u_{w\,air}) + c_w \quad (11)$$

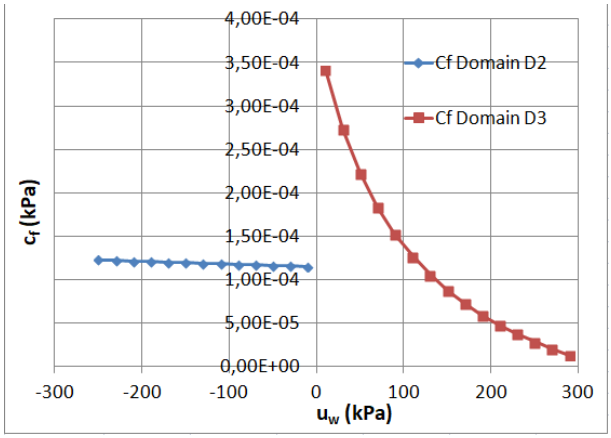

Figure 2. Evolution of the compression coefficient of the interstitial fluid c_f (water + occluded air) calculated with S_{re} = 0.96, S_{rair} = 0.85: for domain D2 (blue curve) with S_r varying between 0.90 and 0.96; for the domain D3 (red curve) with S_r varying between 0.96 and 0.995

2.5.3. Domain D3: the coefficient c_f varies

In the D3 domain, Boutonnier [6] establishes the Eq.ship eq. (12) between water pressure and degree of saturation taking into account Henry's law (dissolution of air in water, h = 0, 02 at 20 ° C) and the ideal gas law. He also considers that occluded air bubbles have a constant capillary radius r_{bm} (approximately close to the largest voids of the soil). These air bubbles are saturated with water vapor (water vapor pressure u_{wg} = 2.3 kPa at 20° C). The capillary radius r_{bm} is most often a few microns with P_a the atmospheric pressure ($P_a \approx$ 101kPa at sea level). The degree of saturation S_{re} is the degree of saturation for a water pressure of zero eq. (12).

The compressibility coefficient of the air + air bubble mixture varies (Fig. 2) in the domain D3 according to eq. (13).

$$S_r = 1/(1 - h + ((1 - S_{re} + h.S_{re}))/ S_{re} . ((s_{bm} + P_a - u_{wg}))/((u_w + s_{bm} + P_a - u_{wg}))) \quad (12)$$

$$c_f = c_w + ((1 - S_r + h.S_r))/(u_w + s_{bm} + P_a) \quad (13)$$

2.6. Theoretical model in effective stress of the expansion of pressuremeter probe

Undrained condition implies the impermeability of the boundaries of the elementary prism used to represent the soil (Fig. 3), but it allows the volume variation by the compressibility of the interstitial fluid and it also allows the variation of the interstitial pressures by the fluid hydrostatics .The quasi-saturated soil theory presented previously will be useful for fine soils where the test is too fast for drainage. The limit is usually set around a permeability of 10^{-8} m /s [11]..

2.6.1. Deformation for a probe in a slice of soil of infinite outer radius

The elementary volume (Fig.3) deforms in the horizontal plane. In the case of small deformations, the variation of volume is the sum of the principal deformations eq. (14), but as one assumes a slice of ground in state of plane strain (Fig. 8) the vertical deformation is null (ε_z= 0). In linear elasticity the deformations ε_r and ε_θ are equal and opposite, the volume variation is zero eq. (14).

$$\varepsilon_v = dV / V_0 = \varepsilon_r + \varepsilon_\theta + \varepsilon_z = (du/dr + u/r) \quad (14)$$

In the case of large deformations the variation of volume dV of the elementary prism is related only to the variation of volume of the voids. It is equal to dV_v whose expression depends on the porosity n and the compressibility coefficient of the interstitial fluid c_w. The negative sign comes the volume decreasing, the interstitial pressure increases. This Eq. is written for the pressuremeter as a variation of volume which is related to the displacement by eq. (14); we can write the equality of the two volume variations eq. (14) and eq. (15) which leads to eq. (16) for a constant c_f. The pore pressure variation eq. (17) is shown to be precise enough to represent the calculated finite element pore pressure.

$$\varepsilon_v = dV / V_0 = -c_f . n . du_w \quad (15)$$

$$u\_w = -1/(c\_f . n) ((u . du)/(r . dr)) + u\_w0 \quad (16)$$

$$du_w = -1/(c\_f . n) . [(u . du)/(r . dr)] \quad (17)$$

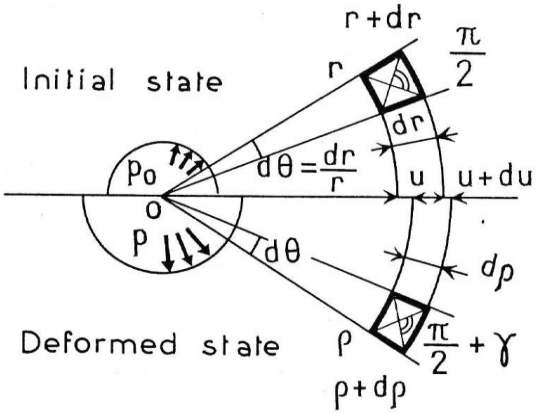

Figure 3. Elemental deformation condition in the horizontal plane by Baguelin [12].

2.6.2. Equations of effective undrained linear elastic equilibrium for infinite radius

The equilibrium condition is given by eq. (18). For a linear elastic modulus there is no volume variation and no increase of pore pressure.

$$\sigma'_r - \sigma'_\theta + r . \sigma'_r/dr + r . du_w/dr = 0 \quad (18)$$

2.6.3. Equations of effective undrained linear elastic equilibrium for finite radius

It is commonly considered that the pressuremeter impacts an outer radius of the soil of the order of 1 to 2m, which represent the no-displacement limit. The outer radius is therefore R_{max}, when the radius of the pressuremeter probe is a, we find the volume of the corresponding circular ring by the equation eq. (19). This

practical method introduces a model-related interstitial pressure eq. (20).

$$V = \pi.(R^2 - r^2).h \quad (19)$$

$$\Delta u_w = -(2.a.u_a)/((R^2 - r^2).n.c_f) \quad (20)$$

For a cylinder whose outer diameter R_{max} is fixed, the general solution is eq. (21)

$$u = C_{1ND}.(1/r - 1/R_{max}) \quad (21)$$

The strains become

$$\varepsilon_r = du/dr = -C_{1ND}/r^2 < 0 \quad (22)$$

$$\varepsilon_\theta = u/r = C_{1ND}/r.(1/r - 1/R_{max}) > 0 \quad (23)$$

The effective stresses are eq. (23) and eq. (24) with λ and μ the Lamé elastic coefficients

$$\sigma'_r = 2.\mu.C_{1ND}/r^2 + \lambda.C_{1ND}/(r.R_{max}) + K_0.\sigma'_z \quad (24)$$

$$\sigma'_\theta = -2.\mu.C_{1ND}/r^2 + (\lambda + 2.\mu).C_{1ND}/(r.R\_max) + K_0.\sigma'_z \quad (25)$$

The total stress at the borehole is (26)

$$\sigma_{ra} = 2.\mu.C_{1ND}/a^2 + \lambda.C_{1ND}/(a.R\_max) + (2.a.u\_a)/((R_{max}^2 - a^2).n.c_f) + K_0.\sigma'_z + u_{w0} \quad (26)$$

The value of the constant C_{1ND} depends of the pressure applied at the borehole wall σ_{ra} and is equal to eq. (27), and the pore pressure varies with the eq.(29)

$$C_{1ND} = (\sigma_{ra} - K_0.\sigma'_z - u_{w0})/[(2.\mu)/a^2 + \lambda/(a.R_{max}) + (2.(R_{max} - a))/(R_{max}.(R_{max}^2 - a^2).n.c_f)] \quad (27)$$

$$u_w = (2.C_{1ND}.(R_{max} - a))/(R_{max}.(R_{max}^2 - a^2).n.c_f) + u_{w0} \quad (29)$$

3. Validation of the undrained unsaturated analytical model

The Finite Elements calculation was performed by Plaxis with the parameters (Table 1) in large deformations. The boundary conditions are in undrained conditions without displacement (Fig. 4) with a borehole of 2.5 cm in diameter, for 15 cm high (in a cylinder of 7.5 cm radius) as for the experiment of Anderson [13]. The mesh used is refined around the borehole (Fig. 4). The parameters used in the calculation are indicated (Table 1). Some parameters (n, E_{oed}, G, K_f, c_{sol}, K_{sol}) are superfluous, but are included in the table for better readability; The calculation allows to check the different hypotheses used in the modeling.

The limit conditions are no displacement for the upper, lower and rigth limit. The pressure p is applied at the borehole wall at the left limit. The comparison of the numerically calculated interstitial pressure with Plaxis and that deduced from eq. (29) when the total pressure at the borehole is increased is indicated for a coefficient B of 0.989 in the case of large deformations (Fig. 5) as well as for a B coefficient of 0.342 in the case of large deformations (Fig. 8).

Table 1. The parameters used in validation with Plaxis - Numerical results EGIS

	unit	Soil A	Soil B
Pressure at borehole	kPa	0 - 100 - 240 - 360	0 - 240 - 360
Radius a	m	0.0125	0.0125
e_0		0,6	0,45
n		0,375	0,310
E	kPa	7428.5	74290
ν		0,3	0,3
E_{oed}	kPa	10000	100000
λ	kPa	4285	42859
G or μ	kPa	2857	28573
K_0		1	1
σ'_z	kPa	0	0
c_f	kPa^{-1}	5.10^{-6}	1.10^{-4}
K_f	kPa	200.10^3	10.10^3
c_{sol}	kPa	200.10^3	10.10^3
$K_{sol} = \lambda + 2/3.\mu$	kPa^{-1}	$1{,}62.10^{-4}$	$1{,}62.10^{-5}$
u_{w0}	kPa	6190	61908
B	kPa	0	0
$R_{ext\ ModèleEF}$		0,984	0,342
$H_{ext\ ModèleEF}$	m	0.15	0.15

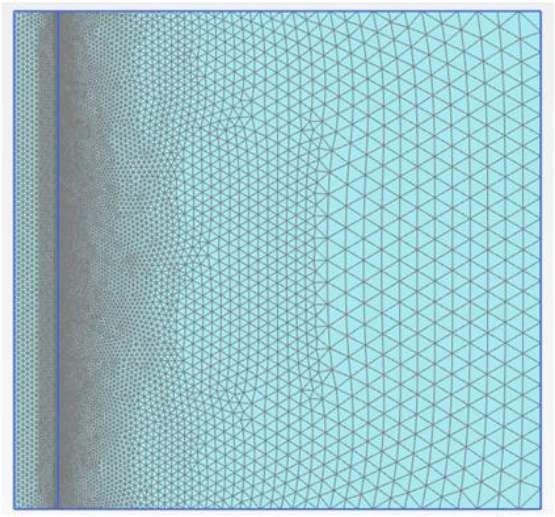

Figure 4. Plaxis mesh used for the Finite Element calculation.

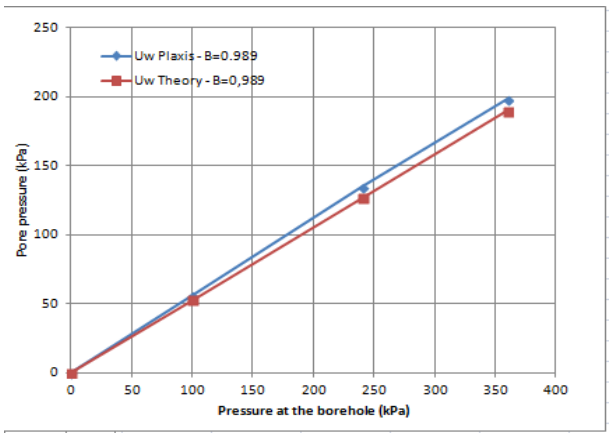

Figure 5. Large Deformation - Comparison of pore pressures at the borehole versus total the total stress applied, B = 0.989.

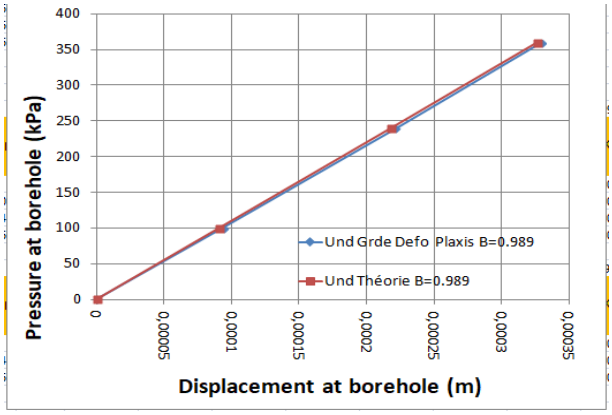

Figure 6. Large Deformation - Comparison of displacements at the borehole versus total the total stress applied, B = 0.989.

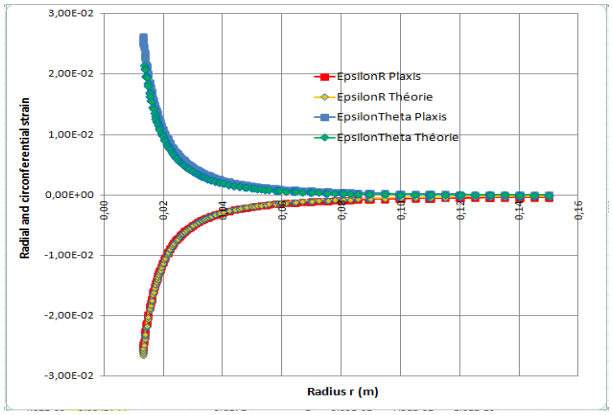

Figure 7. Large Deformation - Comparison of radial and circumferential strains versus the radius, p=360kPa, B = 0.989

We may notice :

- The elastic linearity of the Eq. between the pressure applied to the borehole and the interstitial pressure,
- the small difference between the interstitial pressure calculated numerically by EF and the theoretical result given by the eq.(27)

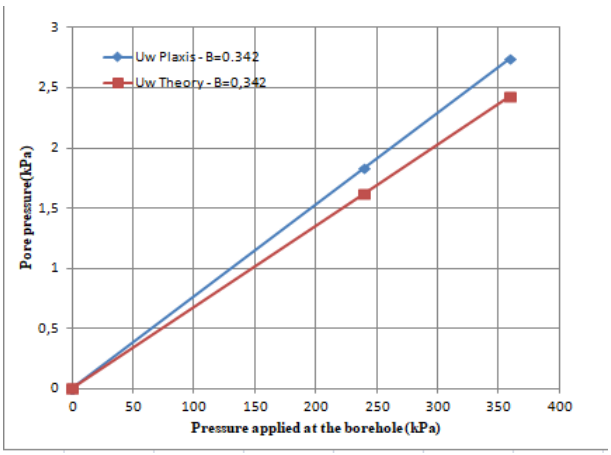

Figure 8. Large Deformation - Comparison of pore pressures at the borehole versus total the total stress applied, B = 0.342.

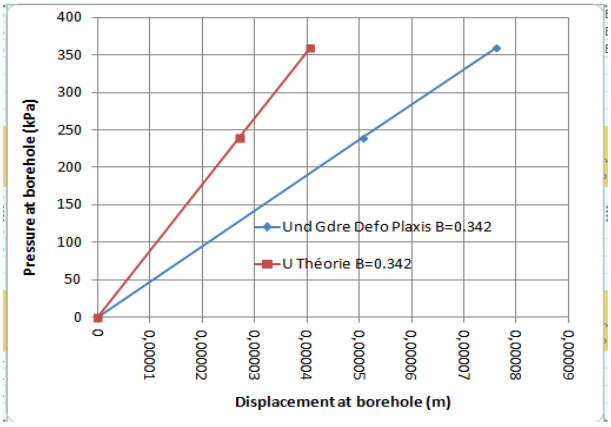

Figure 9. Large Deformation - Comparison of displacements at the borehole versus total the total stress applied, B = 0.342.

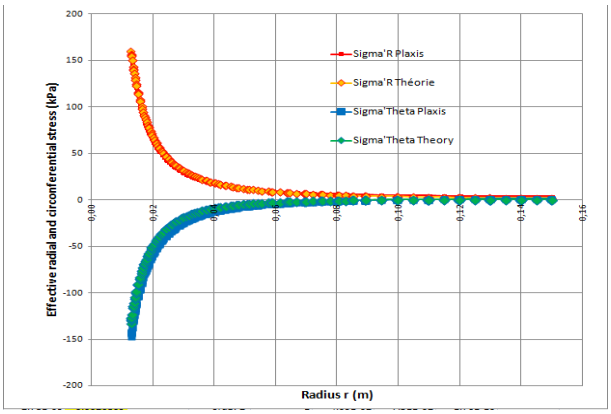

Figure 10. Large Deformation - Comparison of radial and circumferential effective stresses, p=360kPa B = .989

- the great influence of the coefficient B on the value of the interstitial pressure which passes from 200kPa on average for B = 0.989 and 360kPa applied to the drilling at 2.7kPa for B = 0.342 with the same loading at the borehole, which decreases the interstitial pressure with a factor close to 74.

The comparison of the displacements calculated by Plaxis at the borehole and the theoretical displacements given by the eq.(20) shows a good coincidence between

Plaxis calculation and theory for the soil A in large deformation (Fig. 6) while the difference reaches 40% for soil B (Fig. 9).

The comparaison Plaxis versus theory for the strains shows a good agreement either for the radial and circumferential strains (Fig.7). The comparaison Plaxis.

The comparaison Plaxis versus theory for the effective stress also shows a good agreement either for the radial and circumferential strains (Fig.10).

3.1. Theoretical Eq.s

For the pressuremeter, the total radial stress at the borehole is written according to the equation (25) which gives in variation (29); the circumferential deformation to the borehole is written according to equation (22) which gives a variation (30); the ratio of these two quantities is equal to twice the apparent shear modulus which allows to find the apparent Young modulus by eq. (32)

$$\Delta\sigma_r = [(2.\mu.)/a^2 + \lambda/(a.R_{max}) + (2.(R_{max} - a))/(R_{max}.(R_{max}^2 - a^2).n.c_f)]\,\Delta C_{1ND} \quad (29)$$

$$\Delta\varepsilon_\theta = \Delta u/a = [1/a^2 - 1/(a.R_{max})]\,\Delta C_{1ND} \quad (30)$$

$$2.G_{ap} = E_{ap}/(1+\nu) \quad (31)$$
$$= [(2.\mu.)/a^2 + \lambda/(a.R_{max}) + (2.(R\_max - a))/(R_{max}.(R_{max}^2 - a^2).n.c_f)]/[1/a - 1/R_{max}].a$$

$$E_{ap} = [(2.\mu.)/a^2 + \lambda/(a.R_{max}) + (2.(R\_max - a))/(R_{max}.(R_{max}^2 - a^2).n.c_f)]/[1/a - 1/R_{max}].a.(1+\nu) \quad (32)$$

The Eq.ship between the apparent Elastic Module E_{ap} and Young's modulus E can be considered (33):

$$E_{ap}/E = [(2.\mu.)/a^2 + \lambda/(a.R_{max}) + (2.(R\_max - a))/(R_{max}.(R_{max}^2 - a^2).n.c_f)]/[1/a - 1/R_{max}].a. \quad (33)$$

Introducing the value of B_{pres} eq.(34) in eq.(33) and choosing R_{ap} as the ratio between R_{max} (limit of the pressuremeter influence) and a (borehole radius) leads to eq. (35) for the theoretical ratio between apparent and effective Young modulus.

$$B_{pres} = 1/(1 + c_f.n.E_{oed}) \quad (34)$$

$$E_{ap}/E = R_{ap}/(R_{ap}-1)\,[1 + \nu/(R_{ap}.(1 - 2.\nu)) + (2.(1-\nu).(R_{ap} - 1))/((1-2.\nu).R_{ap}.(R_{ap}^2 - 1)).B_{pres}/(1 - B_{pres})] \quad (35)$$

3.2. Numerical applications

Considering the values of (Table 2) and the ratio $R_{ap}=R_{max}/a$ equal to 12, Fig.11 is drawn. It can be see:

- the overestimation ratio depends only on three variables ν, E_{pres} and R_{ap}
- the closer the B_{pres} coefficient is to 1, the greater the overestimation of the Young's modulus of the soil is.
- the less is the effective Young's modulus, the more is the overestimation ratio, but remaining on the same general curve (see blue curve, Fig.11). For modules greater than or equal to 100 MPa, there is small overestimation (see yellow curve, Fig.11).

.

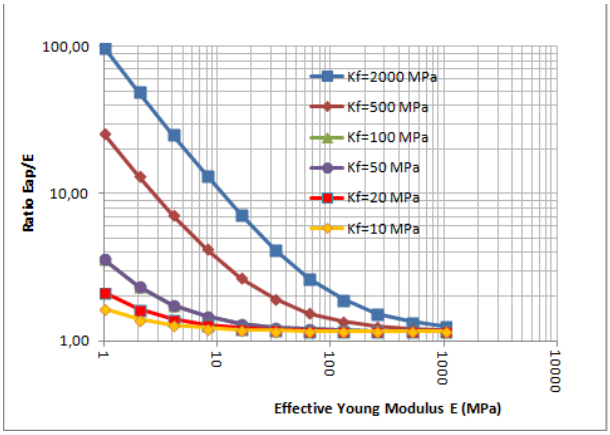

Figure 11. Overestimation factor of Young's modulus of soil as a function of E; for different degree of saturation Sr; u_w = + / - 1000kPa; ν = 0.3.

4. Conclusions

This study has shown the following points:

- The calculation of the undrained and unsaturated hydro-mechanical equilibrium (domain D2 and D3) with a linear elasticity has been solved in small deformations and large displacements for a system with finite or infinite limit conditions
- The assumption of linear elasticity leads to the first order a uniform distribution of interstitial pressure along the radius
- The model shows that the linear elastic resolution in a volume of soil of infinite dimension is of no practical interest because there is no variation of the pore pressure:
- For large deformations, the Plaxis calculation shows that the variation of pore pressure is of second order and can be neglected; as the shear deformations are symmetrical, the interstitial pressure does not vary.
- For small deformations, the volume variation is zero and the pore pressure does not vary

The main interesting case is for the test carried out in a soil of finite dimensions R_{max}.

- For large deformations, the volume variation is of the second order and can be neglected in front of the variation in average soil volume.
- For small deformations in finite shows the existence of strong variations of interstitial pressures related to the variation of average volume of the soil around the pressuremeter.
- The overestimation of the Young modulus can reach a factor of 100 from the effective Young modulus, mainly depending on the value of the compressibility coefficient of the mixture water+air.

The perspectives of this research are studying:

Table 2 : Parametric study of the effect of B coefficient

B	B_{pres}	e	n	E Mpa	E_{oed} MPa	c_f MPa-1	$K_f = c_f^{-1}$ Mpa	K_{sol} Mpa	E_{ap} Mpa
0,999	0,998	0,60	0,375	7	10	5,00E-04	2000	6,2	105,58
0,989	0,982	0,60	0,375	7	10	5,00E-03	200	6,2	18,31
0,896	0,842	0,60	0,375	7	10	5,00E-02	20	6,2	9,58
0,812	0,727	0,60	0,375	7	10	1,00E-01	10	6,2	9,10
0,683	0,571	0,60	0,375	7	10	2,00E-01	5	6,2	8,85
0,463	0,348	0,60	0,375	7	10	5,00E-01	2	6,2	8,71
0,342	0,244	0,45	0,310	74	100	1,00E-01	10	61,9	86,69

- The suction generated after drilling which will allow to estimate the drilling's stability
- The comparison of the effective modulus to the apparent modulus calculated in total stress which should be as a function of B and the amount of occluded air
- The Non-Linear elasticity hypothesis which should allow a more realistic analysis with the possibility of a mean stress variation and consequently a more significant interstitial pressure variation along the radius, as observed on experiments

Acknowledgement

The project presented in this article is supported by The French National Project ARSCOP

5. References

[1] AFNOR, 2015. NF EN ISO 22476-4 Essai pressiométrique Ménard. AFNOR, Reconnaissance et essais géotechniques.
[2] AFNOR, 2013. NF P94-261 Justification des ouvrages géotechniques - Normes d'application nationale de l'Eurocode 7 - Fondations superficielles - Calcul géotechnique.
[3] Carter, J., Booker, J.R., Yeung, S.K., 1986. Cavity expansion in cohesive frictional soils. Géotechnique 36, 349–358
[4] Monnet, J., Chemaa, T., 1994. Etude théorique et expérimentale de l'équilibre élasto-plastique d'un sol cohérent autour du pressiomètre. Revue Française de Géotechnique 15–26.
[5] Cao, L.F., Teh, C.I., Chang, M.F., 2001. Undrained cavity expansion in modified Cam clay I: Theoretical analysis. Géotechnique 51, 323–334.
[6] Boutonnier, L., 2007b. Comportement hydromécanique des sols fins proches de la saturation. Cas des ouvrages en terre : coefficient B, déformations instantanées et différées, retrait / gonflement. Thèse INPG Grenoble.
[7] Boutonnier L., Bufalo M., Dubreucq T., Fry J-J, Lejeune J.-M., Mahmutovic D. (2019). Conception et construction des ouvrages en sols fins. Sous la coordination de L. Boutonnier. 512 pages. Presses des Ponts (ISBN : 9782859785222).
[8] Therzaghi, K., 1943. Theoretical soil mechanics, John Wiley and Sons. ed.
[9] Skempton, A.W., 1954. The Pore-Pressure Coefficients A and B | Géotechnique. Géotechnique 4, 143–147
[10] Mahmutovic, D., 2016. Etude du comportement des sols proches de la saturation – validation numérique sur essais de laboratoire et ouvrages en terre, Laboratoire 3SR. ed. Université de Grenoble Alpes, Grenoble.
[11] Cambou, B., Bahar, R., 1993. Utilisation de l'essai pressiométrique pour l'identification de paramètres intrinsèques du comportement d'un sol. Revue Française de Géotechnique 63, 39–50.
[12] Baguelin, F., Jezequel, J.F., Shields, D.H., 1978. The pressuremeter and foundation engineering,. Trans Tech Publications, Aedermannsdorf, Switzerland.
[13] Anderson, W.F., Pyrah, I.C., Ali Faisal, H., 1987. Rate effects in Pressuremeter tests in clays. Journal of Geotechnical Engineering, ASCE 113, 1344–1358.